Flow around a square-section cylinder using $k-\omega$ SST delayed detached-eddy simulation

Mary C. Bautista, Jörn Nathan, Hugo Olivares-Espinosa,
Louis Dufresne, and Christian Masson

Département de génie mécanique, École de technologie supérieure,
1100, rue Notre-Dame Ouest, Montréal, QC, H3C 1K3, Canada.

Email: *mary.bautista.1@ens.etsmtl.ca*

ABSTRACT

The advancement in computational resources has played an exceptional role in the development of turbulence modelling. However, the simulation of complex flow is still a challenge if accuracy and low computational cost are needed. Hybrid models originate as an attempt to solve this problem. Their main principle is to use a Reynolds-Averaged Navier-Stokes (RANS) model to solve the near-wall flow and Large-Eddy Simulations (LES) to model the flow behaviour away from walls, particularly in regions of complex phenomena such as flow separation. A turbulence model based on the $k-\omega$ SST RANS approach and on the Delayed Detached-Eddy Simulation (DDES) hybrid technique is employed in this study. The $k-\omega$ SST-DDES model was implemented in OpenFOAM® v2.1.0 and tested. The main objective is to establish a suitable turbulence model that could yield accurate and reliable results for industrial and other practical applications. In order evaluate the proposed model, the flow behaviour around a square-section cylinder is modelled and compared against experimental data. The simulation of this benchmark needs some refinements, nevertheless, the $k-\omega$ SST-DDES model shows promising results.

1 INTRODUCTION

In applied simulations of turbulent flows, RANS models are regularly used since they are reasonably easy to implement and their computational cost is relatively low. Conversely, Large-Eddy Simulation (LES) models provide a more complete description of the flow but at a much higher computational cost. LES models have been shown to accurately reproduce the turbulent field providing that the selection of the filter (shape and width) and the subgrid scale model allow for the reproduction of the dynamically important fluctuations whilst reproducing the effects of the dissipative eddies [1]. While LES models are one of the best alternatives for turbulence modelling, the high computational cost of these type of simulations excludes them from some practical applications (e.g. wind energy, micro-scale atmospheric flow simulations, etc.). However, a compromise between the required accuracy and affordable simulations can be achieved by the use of hybrid models.

Detached-Eddy Simulation (DES) is a hybrid technique that aims at accurately modelling high-Reynolds flows with massively separated zones [2] at a reasonable computational cost. The concept is to solve the boundary layer using a RANS model while using an LES approach outside of it, specially in separated and more complex flow regions [3].

The main disadvantage of DES is the prediction of unphysical separation regions in certain type of grids [4]. If the grid refinement close to the wall exceeds a critical value of approximately $h_{max}/\delta < 0.5$ to 1, where h_{max} is the maximum cell edge length and δ is the local thickness of the boundary layer, the DES approach switches from a RANS to LES inside the boundary layer [5]. Then, the switch does not allow for the generation of sufficient flow instabilities to produce the correct resolved Reynolds stresses for LES. This unwanted phenomena, known as Model Stress Depletion (MSD), causes an artificial separation region or grid-induced separation (GIS) [6]. Delayed Detached-Eddy Simulation (DDES) is a solution proposed to overcome the GIS problem in DES. It essentially delays the switch from RANS to LES using shielding functions [7].

DES and DDES were originally proposed using Spalart-Allmaras as the RANS model [8] and it continues to be the most cited approach. However, in this study a DDES based on the $k-\omega$ SST (Shear Stress Transport) RANS model is employed. Unlike other RANS models, $k-\omega$ SST yields favourable results in adverse pressure zones and in regions of separation [4]. In addition, $k-\omega$ SST can be integrated throughout the flow, including the viscous sublayer; thus, it only requires Dirichlet boundary conditions at the wall [9]. The present development attempts to exploit the advantages of the DDES approach and $k-\omega$ SST model to attain an accurate and less computationally expensive turbulence model for practical (industrial) applications with a massive flow separation.

2 MODEL DESCRIPTION

The flow in the $k-\omega$ SST-DDES model is described by the modified Navier-Stokes equations

$$\frac{\partial \overline{u}_i}{\partial t}+\frac{\partial \overline{u}_i\overline{u}_j}{\partial x_j}= -\frac{1}{\rho}\frac{\partial \overline{p}}{\partial x_j}+\frac{\partial}{\partial x_j}\left[(\nu+\nu_t)\left(\frac{\partial \overline{u}_i}{\partial x_j}+\frac{\partial \overline{u}_j}{\partial x_i}\right)\right] \quad (1)$$

$$\frac{\partial \overline{u}_i}{\partial x_i}=0 \quad (2)$$

where in the RANS-regions $\overline{u}_i$ indicates the time-average velocity, while in the LES-regions $\overline{u}_i$ represents the filtered velocity [10]. This notation applies as well for the pressure p. Additionally, ν_t represents the eddy-viscosity.

This hybrid model uses the same closure equations as the $k-\omega$ SST model (For a detailed description, see [4][1]). The only difference being the introduction of a universal length scale as $\tilde{l}=k^{1/2}/(\beta^*\omega)$ in the equation of the turbulent kinetic energy. Thus, the resulting equations for the turbulent kinetic energy k and the dissipation rate per unit of turbulent kinetic energy ω are [5]

$$\frac{\partial k}{\partial t}+\frac{\partial \overline{u}_j k}{\partial x_j}-\frac{\partial}{\partial x_j}\left[(\nu+\sigma_k\nu_t)\frac{\partial k}{\partial x_j}\right]=\tilde{P}-\frac{k^{3/2}}{\tilde{l}} \quad (3)$$

$$\frac{\partial \omega}{\partial t}+\frac{\partial \overline{u}_j \omega}{\partial x_j}-\frac{\partial}{\partial x_j}\left[(\nu+\sigma_\omega\nu_t)\frac{\partial \omega}{\partial x_j}\right]= \alpha\nu_t\tilde{P}-\beta\omega^2+2(1-F_1)\frac{\sigma_\omega^2}{\omega}\frac{\partial k}{\partial x_j}\frac{\partial \omega}{\partial x_j} \quad (4)$$

[1] As mention in *http://turbmodels.larc.nasa.gov/sst.html* a typographical error exists in the turbulent dissipation equation (Eq. 1) of this article. However, future articles that cite this reference use the corrected equation (e.g. [5]).

As in the $k-\omega$ SST model, the production term $P=2\nu_t S_{ij}S_{ij}$ is delimited by

$$\tilde{P}=\min(P,10\beta^* k\omega) \quad (5)$$

to inhibit the accumulation of turbulence in stagnation regions [4]. Here, $S_{ij}=\frac{1}{2}(\frac{\partial u_i}{\partial x_j}+\frac{\partial u_j}{\partial x_i})$ is the strain rate tensor. The blending functions are given by

$$F1=\tanh\left(arg_1^4\right), \quad (6)$$

$$arg_1=\min\left(\max\left(\frac{\sqrt{k}}{\beta^*\omega d_\omega},\frac{500\nu}{d_\omega^2\omega}\right),\frac{4\rho\sigma_{\omega 2}k}{CD_{k\omega}d_\omega^2}\right), \quad (7)$$

$$CD_{k\omega}=\max\left(2\rho\sigma_{\omega 2}\frac{\nabla k\cdot\nabla\omega}{\omega},10^{-10}\right), \quad (8)$$

$$F2=\tanh\left(arg_2^2\right), \quad (9)$$

$$arg_2=\max\left(\frac{2\sqrt{k}}{\beta^*\omega d_\omega},\frac{500\nu}{d_\omega^2\omega}\right), \quad (10)$$

$$\alpha=\alpha_1 F_1+\alpha_2(1-F_1). \quad (11)$$

The switch between the RANS and the LES modes is introduced in the turbulence model equations using the length scale of the DDES approach [7]. This method is based on DES where the switch is performed using $\tilde{l}_{DES}=\min(l_{RANS},l_{LES})$ [8]. However, to prevent GIS, an empirical shielding function f_d was introduced to act as a second condition to delay the switch inside the boundary layer, thus

$$f_d=1-\tanh\left(C_{d1}r_d\right)^{C_{d2}}. \quad (12)$$

The original formulation of f_d was proposed using the Spalart-Allmaras turbulence model with the value of the constants set to $C_{d1}=8$ and $C_{d2}=3$ [7]. However, a recalibration was done for the $k-\omega$ SST yielding a value of $C_{d1}=20$ and $C_{d2}=3$ [5], which are used here. Furthermore, the function r_d is defined as [7]

$$r_d=\frac{\nu+\nu_t}{\kappa^2 d_w^2\sqrt{\frac{\partial \overline{u}_i}{\partial x_j}\frac{\partial \overline{u}_i}{\partial x_j}}} \quad (13)$$

where κ is the von Karman constant and d_w is the distance perpendicular to the wall. This function equals 1 close to the wall and decreases to 0 as it approaches the edge of the boundary layer. Consequently, $f_d\sim 0$ inside the boundary layer, and $f_d\sim 1$ far away from the wall.

The DDES length scale $\tilde{l}$ used in Eq. 3 is given by [11]

$$\tilde{l}\equiv l_{RANS}-f_d\max(0,l_{RANS}-l_{LES}) \quad (14)$$

which is an adaptation of the original formulation proposed by Spalart [7] to account for any eddy-viscosity

models. In the present, $k-\omega$ SST DDES model the length scales are defined as

$$l_{RANS} = \frac{\sqrt{k}}{\beta^* \omega} \tag{15}$$

$$l_{LES} = C_{DES}\Delta \tag{16}$$

for the RANS-mode [12] and the LES-mode [8] respectively. Additionally

$$C_{DES} = (1-F_1)C_{k-\varepsilon} + F_1 C_{k-\omega} \tag{17}$$

where F_1 is the already known blending function, $\Delta = (\Delta_x \Delta_y \Delta_z)^{1/3}$ is the filter width, and $C_{k-\varepsilon}$ and $C_{k-\omega}$ are constants [12].

The eddy-viscosity is determined for both, the RANS-mode and LES-mode by

$$\nu_t = \frac{a_1 k}{\max(a_1 \omega, \mathcal{S} F_2)} \tag{18}$$

where $\mathcal{S} = \sqrt{S_{ij} S_{ij}}$ is the characteristic strain rate. Finally, all the $k-\omega$ SST-DDES model constants are given in Table 1.

Table 1: $k-\omega$ SST-DDES turbulence model constants.

$\alpha_1 = 5/9$	$\alpha_2 = 0.44$	$a_1 = 0.31$
$\beta_1 = 0.075$	$\beta_2 = 0.0828$	$\kappa = 0.41$
$\sigma_{k1} = 0.85$	$\sigma_{k2} = 1$	$\beta^* = 0.09$
$\sigma_{\omega 1} = 0.5$	$\sigma_{\omega 2} = 0.856$	
$C_{k-\varepsilon} = 0.61$	$C_{k-\omega} = 0.78$	
$C_{d1} = 20$	$C_{d2} = 3$	

The ability of this model to accurately reproduce the transfer of turbulent kinetic energy from the large to the small eddies has been verified by a simulation of decaying isotropic turbulence. Thus, an initial turbulent field was modelled in a cubic domain with only periodic boundaries. Due to the absence of a boundary layer in this case, the simulation ran always in LES-mode. The $k-\omega$ SST-DDES model (using the proposed constants) has been validated against the decaying isotropic turbulence experiment of Comte-Bellot and Corrsin [13], and against simulations of the standard Smagorinsky LES model. Results from these tests show a good agreement as seen in Figure 1. The choice of interpolation scheme may have an impact on the simulations, especially in the dissipative ranges. Likewise, a test to validate the coupling with the RANS mode is being established.

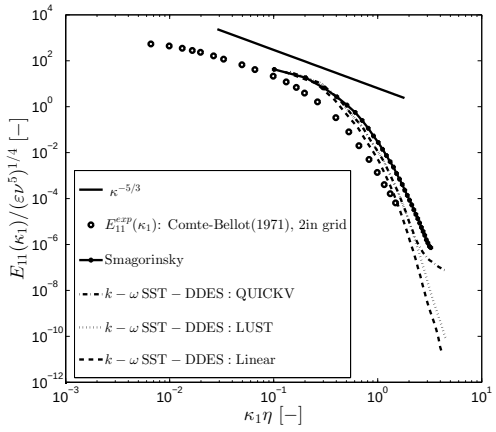

Figure 1: Spectra of decaying isotropic turbulence. Experimental data taken from [13]. The plot labels represent the interpolation schemes used for the convection term of the velocity.

3 SIMULATION OF THE FLOW AROUND A SQUARE-SECTION CYLINDER

The flow around a square-section cylinder presents complex phenomena (i.e. flow separation and reattachment, formation of a wake, vortex shedding, interaction with the wall, etc.) which pose many challenges for numerical simulations. A global good agreement between experimental results and simulations has not been achieved by any turbulence model [14]. Hence, this case provides an ambitious benchmark to test the behaviour of the newly implemented $k-\omega$ SST-DDES model.

A detailed analysis of the turbulent flow around a square-section cylinder was carried out to mimic the data of CFD Society of Canada 2012 Challenge experiment (http://www.cfdcanada.ca/challenge) using OpenFOAM® v2.1.0. A square cylinder with a side cross-section of $d = 12.7$mm and a height of $h = 50.4$mm (aspect ratio $h/d \approx 4$) represents the obstacle. The dimensions of the numerical domain are $(L_x, L_y, L_z) \approx (7.25h, 2.15h, 1.75h)$ which represent the streamwise, spanwise and vertical directions, respectively. The grid has approximately $8 \cdot 10^5$ cells. Considering that the aim of this study is to model the turbulent flow in the perspective of low computational cost simulations, a relatively small size domain with a small number of cells was used.

Based on the recommended gridding guidelines for DES [15], two important aspects were considered for the mesh refinement. First, most of the cells are ap-

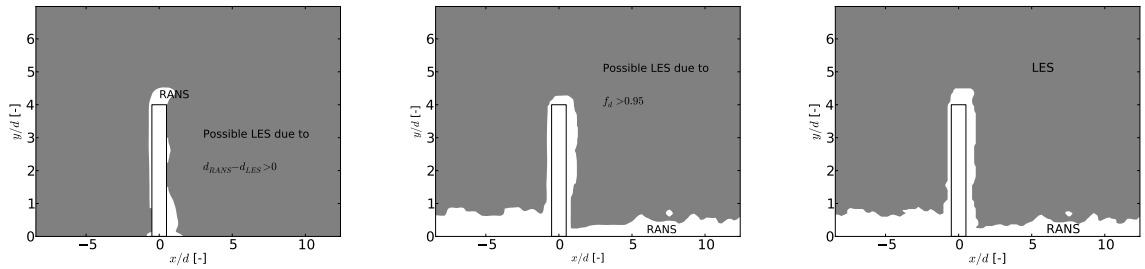

(a) $l_{RANS} - l_{LES}$ term from Eq. 14 (b) f_d from Eq. 12 (c) LES/RANS regions

Figure 2: Visualization the different parameters that determine the LES regions (grey) and RANS regions (white) at a particular t_0 in the $y = 0$ plane.

proximately cubic. Secondly, the cells close to the wall are refined in the vertical direction to obtain a $z_1^+ = z_1 u_* / \nu \approx 1$ as required by $k-\omega$ SST. Here, z_1 is the location of the first cell close to the wall and u_* is the friction velocity. As in LES, the grid convergence of a hybrid model is not a straightforward process. A thorough convergence test is being considered at the present time.

As in the experiment, the simulated flow is characterized by a free-stream velocity U_∞ of 15 m/s, and an unperturbed boundary layer with a height of $0.18h$. Furthermore, the Reynolds number is $U_\infty d/\nu = 11\,000$, and the free stream turbulence intensity is approximately 1%. The simulation ran for 50 flow-through-times (U_∞/L_x) to allow for the turbulence to properly develop. Then, the time averaged values and other relevant statistics were calculated for approximately another 50 flow-through-times. A CFL number of 0.5 was used throughout.

The modelled upstream region has a length of $4h$. The inlet boundary condition is obtained by mapping the plane located at a distance h from the leading edge on to the inlet in every time step and for all the variables. This is analogous to a precursor simulation which is used to map the output results as an unsteady inlet for the obstacle simulation. It was verified that the obstacle influence did not reach the plane located at h from the inlet. The internal field was initialized with a logarithmic velocity profile within the boundary layer with added random fluctuations. A no-slip boundary condition was imposed at the bottom and on the obstacle without any wall function. The values of k and ω at the walls (bottom and obstacle) where defined following the recommendations for the $k-\omega$ SST model [16]. Finally, a convective outflow boundary condition is imposed at the top, outlet and lateral faces, such that

$$\frac{\partial \phi}{\partial t} + U_n \frac{\partial \phi}{\partial n} = 0, \tag{19}$$

for any variable ϕ in the direction n normal to the boundary [17]. The convective boundary prevents unphysical behaviour by allowing the flow exit the domain freely. Similarly, nothing prevents the flow to enter the domain.

The choice of numerical schemes for a hybrid model is difficult due to the contradicting requirements for LES and RANS. Central schemes are recommended for LES simulations because they are less dissipative. However, they are generally not stable for RANS. On the other hand, the more stable upwind schemes used in RANS simulations are too dissipative to use in LES [12]. Several schemes were tested as part of this analysis. Based on Figure 1 and on the stability of the square cylinder simulations, the interpolation scheme Linear-Upwind Stabilized Transport (LUST) was used for the convective term of the velocity. LUST is an OpenFOAM® second-order interpolation scheme that blends linear-upwind and linear schemes to make the solution more stable [18]. For stability purposes, upwind schemes were used for the divergence and gradient terms of k and ω. A future analysis of this turbulence model will include hybrid schemes as the one proposed by Travin *et al.* [12]. This hybrid scheme switches from a central scheme in the LES regions to an upwind scheme in the RANS mode. Lastly the temporal derivative is solved using a second-order implicit scheme.

4 RESULTS

An initial assessment for any hybrid model should include the verification of the switch that determines the RANS and LES zones. Figure 2 shows a snapshot at a particular time of the parameters that regulate this switch. The desired behaviour is successfully being reproduced since RANS regions are present near the walls, while away from the wall and especially in the wake zone, the LES mode is being applied.

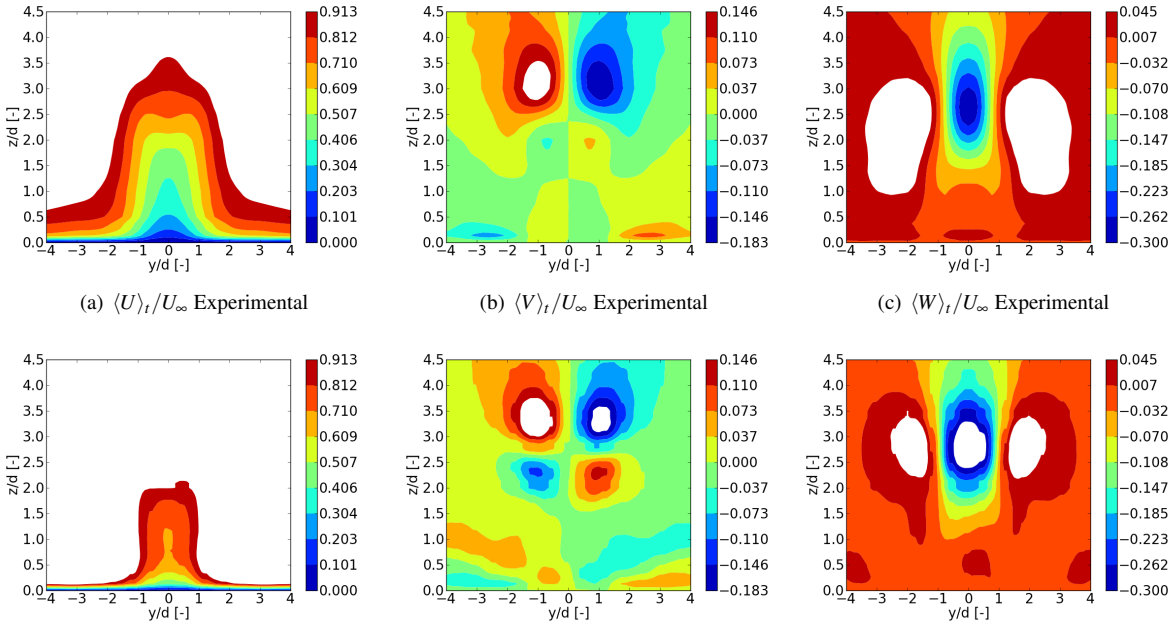

(a) $\langle U \rangle_t / U_\infty$ Experimental (b) $\langle V \rangle_t / U_\infty$ Experimental (c) $\langle W \rangle_t / U_\infty$ Experimental

(d) $\langle U \rangle_t / U_\infty$ Modelled (e) $\langle V \rangle_t / U_\infty$ Modelled (f) $\langle W \rangle_t / U_\infty$ Modelled

Figure 3: Comparison of the time averaged mean velocity $\langle U_i \rangle_t$ at a plane $x = 5d$ from the obstacle center.

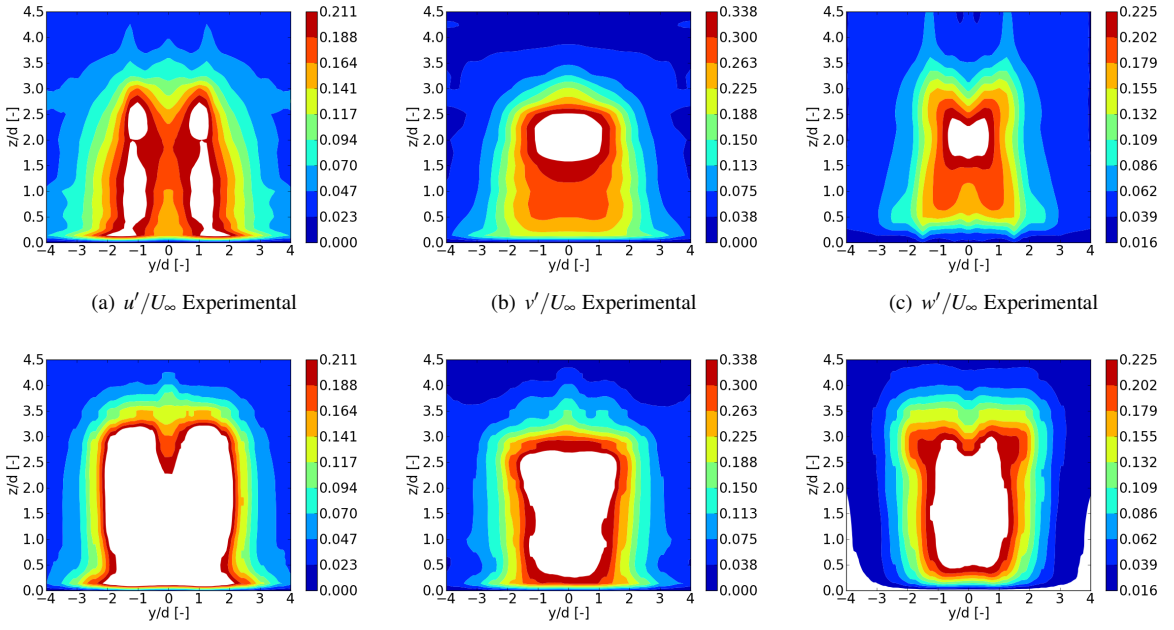

(a) u'/U_∞ Experimental (b) v'/U_∞ Experimental (c) w'/U_∞ Experimental

(d) u'/U_∞ Modelled (e) v'/U_∞ Modelled (f) w'/U_∞ Modelled

Figure 4: Comparison of the time averaged velocity fluctuations defined as $u_i' = U_i - \langle U_i \rangle_t$ at a plane $x = 5d$ from the obstacle center.

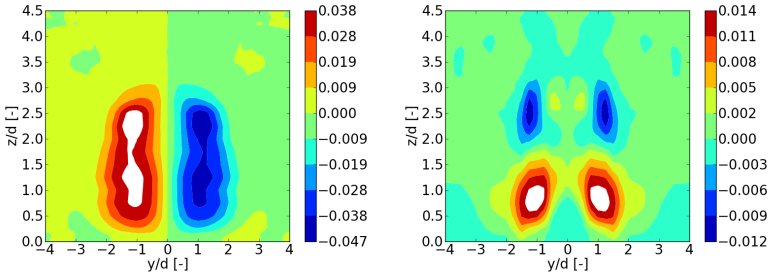

(a) $u'v'/U_\infty^2$ Experimental (b) $u'w'/U_\infty^2$ Experimental

(c) $u'v'/U_\infty^2$ Modelled (d) $u'w'/U_\infty^2$ Modelled

Figure 5: Comparison of the time averaged Reynolds Stresses $u_i'u_j'$ at a plane $x = 5d$ from the obstacle center.

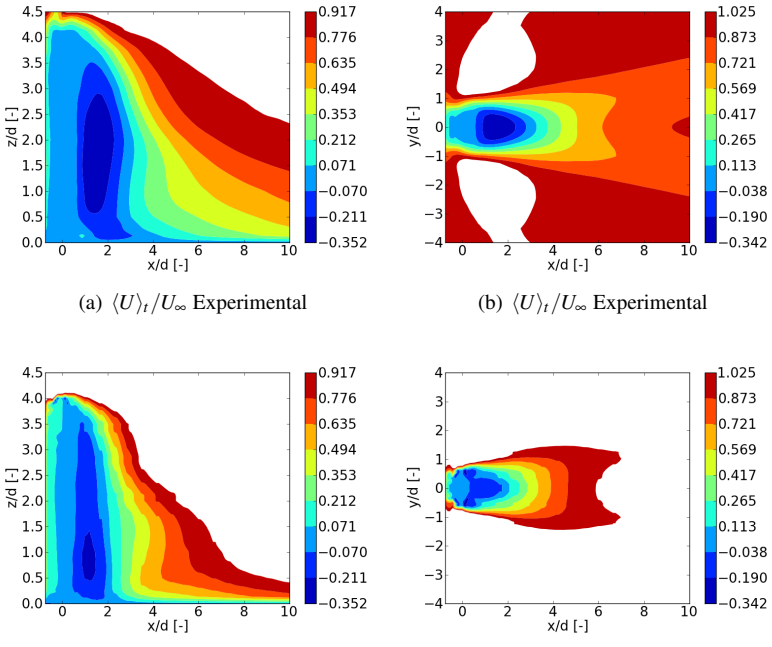

(a) $\langle U \rangle_t / U_\infty$ Experimental (b) $\langle U \rangle_t / U_\infty$ Experimental

(c) $\langle U \rangle_t / U_\infty$ Modelled (d) $\langle U \rangle_t / U_\infty$ Modelled

Figure 6: Comparison of the time averaged mean velocity $\langle U_i \rangle_t$ for (a) and (c) at a plane $y = 0$ and for (b) and (d) at a plane $z = 2d$.

The time average data can be seen in Figures 3 - 5 at a plane $x = 5d$ from the obstacle center. The data obtained at different distances downstream from the obstacle was analyzed (not shown). In addition, the time averaged mean velocity at the middle vertical plane and at the horizontal plane $z = 2h$ is compared and shown in Figure 6. In all horizontal, vertical and transversal planes the numerical and experimental results present a good qualitative agreement overall. However, an important discrepancy can be seen in the order of magnitude of all the variables.

To better understand and visualize this problem, the numerical and experimental results for the time averaged velocity profiles are compared on Figure 7 for a vertical plane at $y = 0$ and on Figure 8 for a horizontal plane at $z = d$. Once more, there is a qualitative agreement of the data, but the value of the mean velocity is overestimated. Preliminary investigation of this problem has not led to a significant explanation yet.

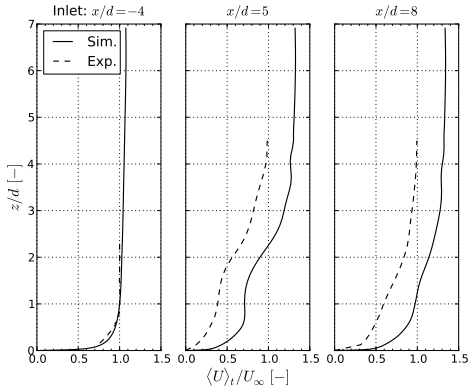

Figure 7: The time averaged velocity profiles at different distances from the obstacle at $y = 0$

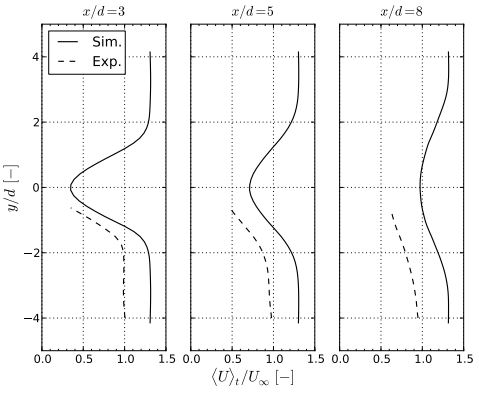

Figure 8: The time averaged velocity profiles at different distances from the obstacle at $z = d$

The complexity of the wake can be observed in Figure 9. Furthermore, in Figure 10 vorticity contour plot shows clearly the vortex formation and shedding behind the square cylinder. The period of the vortex shedding was analyzed using the lift coefficient c_l shown in Figure 11. This value is calculated by $c_l = F_l/(\rho U_\infty^2 A/2)$ where F_l is the lateral lift force and A is the cross-section area of the cylinder. Also, it was verified that the time average of c_l was $3.1 \cdot 10^{-6}$. The measured average period is $t_p \approx 0.008$ s. This corresponds to a Strouhal number of 0.106 based on U_∞ and d. Other experiments have found that for square cylinders with an aspect ratio of 4 and a Reynolds number in the order of 10^4 the Strouhal number is approximately 0.125 [19] and 0.15 [20] which in consistent with our results.

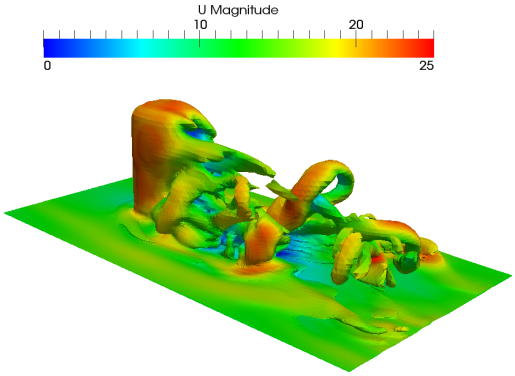

Figure 9: The vorticity structures at the wake.

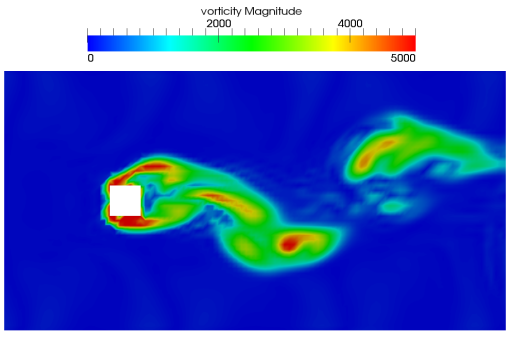

Figure 10: The vortex shedding can be visualized on a vorticity contour plot at the $z \approx 3d$ plane.

5 Conclusion

The hybrid model $k - \omega$ SST-DDES has been implemented in OpenFOAM®v2.0.1 with the objective of delivering a turbulence model that could achieve fairly accurate results at an affordable computational cost. The model validation based on decaying isotropic turbulence simulation showed that the

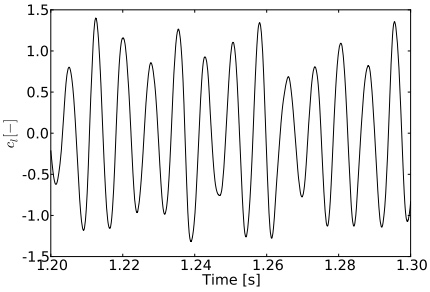

Figure 11: The lift coefficient as a function of time was used to calculate the frequency of the vortex shedding

$k-\omega$ SST-DDES is capable of reproducing the turbulence kinetic energy cascade. These results indicate that the model is suitable for simulating correctly the turbulent flow behaviour. Subsequently, the turbulent flow around a square-section cylinder was studied. The $k-\omega$ SST-DDES model has shown good qualitative agreement with experimental data on a challenging test case. Some discrepancies remain and are under investigation. Nevertheless the present work has shown promising results, and it is expected that with the proper adjustments, accurate and reliable results at an affordable computational cost could be obtained.

ACKNOWLEDGMENTS

The support of Hydro-Québec, the Fonds de recherche du Québec - Nature et technologies (FQRNT), la Chaire de recherche du Canada sur l'aérodynamic des éoliennes en milieu nordique (AEMN), the Natural Sciences and Engineering Research Council of Canada (NSERC) and the Consejo Nacional de Ciencia y Tecnología (CONACYT-México) is greatly appreciated.

REFERENCES

[1] Pope, S. B., *Turbulent Flows* Cambridge University Press, 2000.

[2] Spalart, P. R., Detached-Eddy Simulation, *Annual Rev. Fluid Mech.*, 41:181-202, 2009.

[3] Squires, K.D., Detached-Eddy Simulation: Current Status and Perspectives, in *Direct and Large-Eddy Simulation*, Kluwer Academic Publishers, pp. 465-480, 2004.

[4] Menter, F., Kuntz, M. and Langtry, R., Ten Years of Industrial Experience with the SST Turbulence Model, *Turbulence, Heat and Mass Transfer 4*, 4:625-632, 2003.

[5] Gritskevich, M.S, Garbaruk, A.V, Schütze, J. and Menter, F.R. Development of DDES and IDDES Formulations for the $k-\omega$ Shear Transport Model, *Flow, Turbulence and Combustion*, 88(3):431-449, 2012.

[6] Menter, F. R., Kutz, M. Adaptation of eddy-viscosity turbulence models to unsteady separated flow behind vehicles., *United Engineering Foundation Conference: The Aerodynamics of Heavy Vehicles: Trucks, Buses and Trains*, McCallen, R., Browand, F., and Ross, J. eds. Monterrey, California Dec 2-6 2002, pp. 339-352. Published by Springer in 2004.

[7] Spalart, P. R., Deck, S. et al., A New Version of Detached-eddy Simulation, Resistant to Ambiguous Grid Densities, *Theoretical and Computational Fluid Dynamics*, 20(3):181-195, 2006.

[8] Spalart, P. R et al., Comments on the Feasibility of LES for Wings, and on a Hybrid RANS/LES Approach, *Proceedings of first AFOSR international conference on DNS/LES*, Louisiana Tech University, Ruston, Louisiana, August 4-8, 1997.

[9] Menter, F. R., Improved Two-Equations k-ω Turbulence Models for Aerodynamic Flows *NASA Technical Memorandum* 103975, 1992.

[10] Bechmann, A., *Large-Eddy Simulation of Atmospheric Flow over Complex Terrain*, PhD thesis, Risø National Laboratory. Technical University of Denmark, Roskilde, Denmark, 2007.

[11] Shur, M., Spalart, P., Strelets, M., and Travin, A. A hybrid RANS-LES approach with delayed-DES and wall-modelled LES capabilities., *International Journal of Heat and Fluid Flow*, 29:1638-1649. 2008.

[12] Travin, A., Shur, M. L. Strelets, M. and Spalart, P.R. Physical and numerical upgrades in the detached-eddy simulation of complex turbulent flows., Advances in LES of Complex Flows Conference Proceedings, pp. 239-254, 2002.

[13] Comte-Bellot, G. and Corrsin, S. Simple Eulerian time correlation of full and narrow-band velocity signals in grid-generated, "isotropic" turbulence., *Journal of Fluid Mechanics*, 48(2):273-337. 1971.

[14] Sagaut, P. *Large Eddy Simulations for Incompressible Flows: An Introduction* Springer, 3rd. ed., 2006.

[15] Spalart, P. R., Young-Person's Guide to Detached-Eddy Simulation Grids, *NASA/CR-2001-211032*, July 2001.

[16] Menter, F. R., Zonal Two Equation k-ω Turbulence Models for Aerodynamic Flows, *AIAAJ*, 93:2906, 1993.

[17] Ferzinger, J.H and Perić, M. *Computational Methods for Fluid Dynamics.* 3rd rev. ed. Springer. 2002.

[18] The OpenFOAM Foundation. OpenFOAM v2.0.1: Numerical Methods Web page. *www.openfoam.org/version2.1.0/numerics.php*

[19] Okajima, A. Strouhal numbers of rectangular cylinders J.Fluid Mech. 123:379-398. 1982.

[20] Norberg, C. Flow around rectangular cylinders: Pressure forces and wake frequencies Journal of Wind Engineering and Industrial Aerodynamics, 49:187-196. 1993.